Acta Pharmaceutica Sinica B 2026;16(3):1779−1785

Chinese Pharmaceutical Association
Institute of Materia Medica, Chinese Academy of Medical Sciences

Acta Pharmaceutica Sinica B

www.elsevier.com/locate/apsb
www.sciencedirect.com

LETTER TO THE EDITOR

Distinctive molecular architectures of G_q- and G_i-coupled GLP-1 receptors

KEY WORDS

GLP-1R;
G protein coupling;
Signaling preference;
Cryo-electron microscopy

To the Editor:

The glucagon-like peptide-1 receptor (GLP-1R) plays a central role in glucose homeostasis and energy balance through its activation by the incretin hormone GLP-1[1]. It is highly expressed in pancreatic islets and the gastrointestinal tract, and is also present in the brain and heart[2]. At the signaling level, GLP-1R primarily couples to G_s, activating adenylate cyclase, elevating intracellular cyclic AMP (cAMP), and stimulating PKA/EPAC pathways[3]. Additionally, GLP-1R exhibits pleiotropic coupling to $G_{q/11}$, triggering phospholipase C (PLC) activation and increasing intracellular Ca^{2+} levels (Fig. 1A and B)[4,5]. Under conditions of β-cell membrane depolarization, GLP-1R shifts from G_s to G_q signaling, a mechanism that may underpin the sustained insulinotropic effect of GLP-1 in diabetes[4,5]. Coupling to G_i is less characterized but may contribute to inhibitory feedback or activate alternative signaling cascades in specific cell types[2]. Upon agonist stimulation, GLP-1R is phosphorylated primarily by G protein-coupled receptor (GPCR) kinases (GRKs), which typically promotes recruitment of β-arrestins, thereby facilitating receptor internalization and G protein-independent signaling events such as ERK activation[6-8]. Additionally, recent studies suggest that GLP-1R internalization can occur independently of arrestins, mediated instead through G_s and $G_{i/o}$ activation and GRK phosphorylation[9]. Together, these intracellular signaling pathways—G_s, G_q, G_i, GRK, and β-arrestin—differentially shape the physiological and pharmacological actions of GLP-1R.

Extensive structural biology efforts, including cryo-electron microscopy (cryo-EM) and crystallography, have elucidated the conformational landscape of GLP-1R in complex with G_s across diverse peptide and non-peptide ligands[1,3,10]. However, structural insights into GLP-1R coupled to G_q or G_i remain deficient, hindering a mechanistic explanation of effector selectivity and biased signaling under varying physiological conditions[2,11]. To address this, we determined cryo-EM structures of the human GLP-1R bound to GLP-1 in complex with G_q (2.92 Å) and G_i (3.18 Å) (Fig. 1C and D, Supporting Information Fig. S1−S3, and Table S1). By comparing these structures with that coupled to G_s and integrating functional analysis and molecular dynamics (MD) simulations, we revealed the structural basis of G protein subtype specificity at GLP-1R. Our results provide a structural framework for in-depth understanding of selective signaling at GLP-1R and open avenues for designing tailored therapeutics.

In both the GLP-1−GLP-1R−G_q and GLP-1−GLP-1R−G_i complex structures, the N-terminal segment of GLP-1 made close contact with the transmembrane domain (TMD), while its C-terminal segment formed key interactions with the extracellular domain (ECD), the extracellular tip of transmembrane helix 1 (TM1) and extracellular loop 1 (ECL1) (Fig. 1C and D). Upon comparing the receptor structures, it was noted that the binding modes of GLP-1 in the two complexes were nearly identical, with minor differences observed only in the side-chain orientations of the C-terminal region of GLP-1 and ECL1 of GLP-1R. Structural superposition based on the Cα atoms of the GLP-1R TMD revealed minimal conformational changes in GLP-1R upon binding to different G proteins (Fig. 1E−H), as seen from the Cα root mean square deviation (RMSD) values of the TMD (0.68 Å and 0.73 Å for G_q and G_i, respectively) relative to G_s (PDB code: 6X18)[12]. In contrast, the ECD displayed significantly larger conformational changes, with Cα RMSD values of 1.05 Å and 1.57 Å for G_q and G_i, respectively. Notably, greater conformational variations were observed in the G protein subunits:

Peer review under the responsibility of Chinese Pharmaceutical Association and Institute of Materia Medica, Chinese Academy of Medical Sciences.

https://doi.org/10.1016/j.apsb.2026.01.023

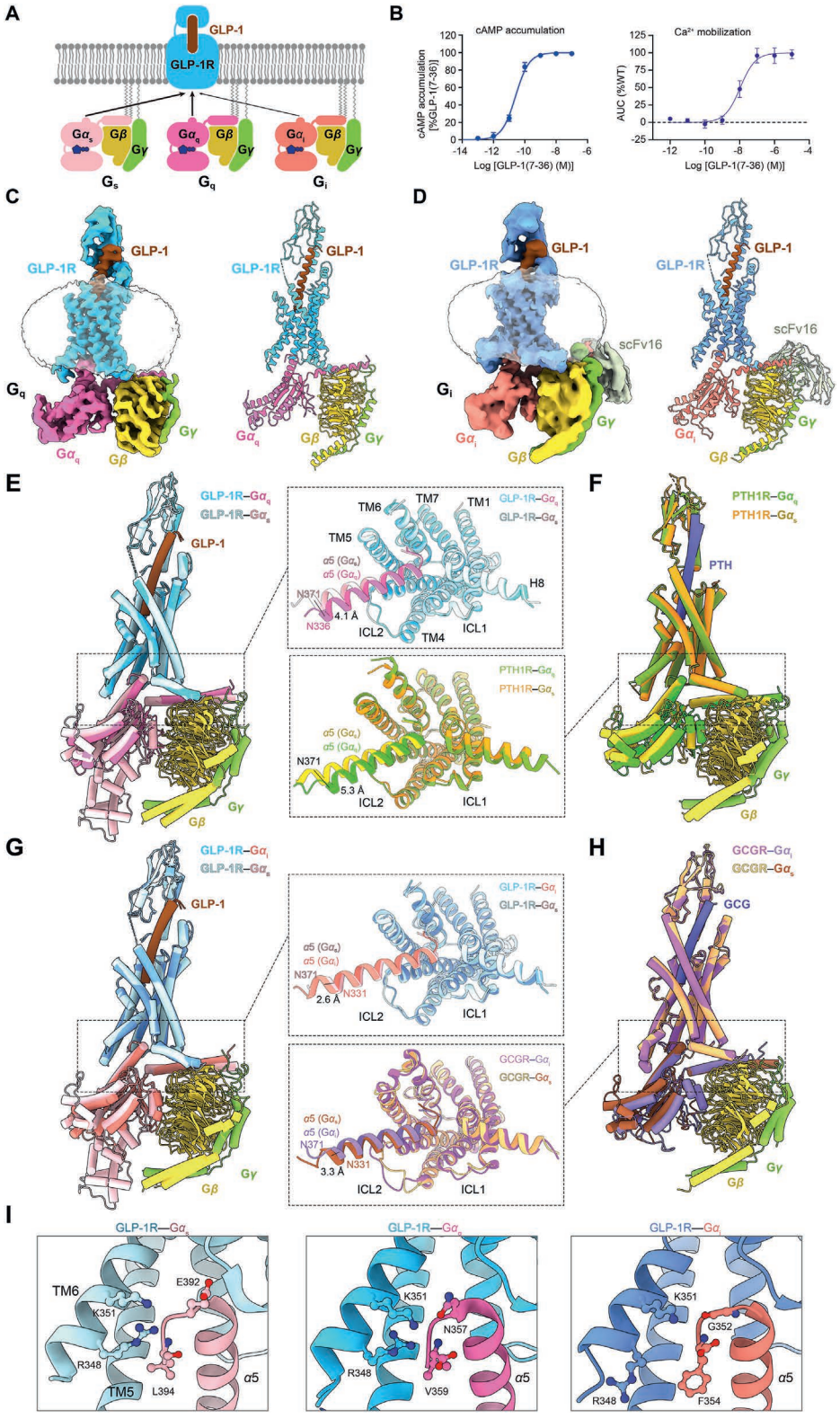

Figure 1 Overall architecture of the GLP-1-bound GLP-1R−G_q and GLP-1R−G_i complexes. (A) Schematic of G protein coupling by GLP-1R. Upon ligand binding, GLP-1R primarily signals through G_s to elevate cAMP levels and engages G_q to increase intracellular Ca^{2+} concentration. (B) Concentration-response curves of GLP-1(7−36)-induced cAMP accumulation (left) and calcium mobilization (right) in HEK293T cells transfected with the human GLP-1R. Calcium mobilization data, shown as area-under-the-curve (AUC), were normalized to buffer (0%) and 1 μmol/L GLP-1(7−36) (100%). Data shown are means ± standard error of mean (SEM) of at least three independent experiments. WT, wild-type. (C) Cryo-EM density map (left) and cartoon representation (right) of GLP-1-bound GLP-1R coupled to G_q. The sharpened cryo-EM density map at the 0.060 threshold shown as light gray surface indicates a micelle diameter of 10 nm. The peptide GLP-1 is shown in saddle brown, GLP-

compared to $G\alpha_s$, $G\alpha_q$ and $G\alpha_i$ showed RMSD values of 2.69 and 2.39 Å, respectively, indicating substantial structural divergence among G protein subtypes (Fig. 1E−H).

Specifically, Gα subunits ($G\alpha_q$, $G\alpha_i$ and $G\alpha_s$) demonstrated distinct conformational rearrangements upon binding to GLP-1R, particularly in the αN and α5 helices. For the αN helix, $G\alpha_q$ showed a global inward shift (Cα distance of 3.04 Å between K10 of $G\alpha_q$ and the equivalent residue K17 of $G\alpha_s$), likely due to different angular orientations relative to the receptor intracellular pocket (Supporting Information Fig. S4A). For the α5 inserted the intracellular crevice of GLP-1R, a bipolar displacement emerged, in which its N-terminal region made notable downward movement (Cα distance of 4.13 Å between N336 of $G\alpha_q$ and N371 of $G\alpha_s$), while its C-terminal tip directly interacting with the TMD remained nearly stationary (Fig. 1E, Fig. S4A). This polarization in the conformation of α5 may reflect a structural adaptation to maintain critical interactions with the receptor while accommodating $G\alpha_q$ positioning. A similar trend was found in GLP-1R-bound $G\alpha_i$ and $G\alpha_s$, where the αN helix and the N-terminal segment of α5 of $G\alpha_i$ exhibited substantial displacements (2.97 and 2.55 Å, respectively) relative to $G\alpha_s$ (Fig. 1G, Fig. S4B). Consequently, the interface areas of GLP-1R−$G\alpha_q$ (1682 Å^2) and GLP-1R−$G\alpha_i$ (1377 Å^2) are markedly smaller than that of the GLP-1R−$G\alpha_s$ (2045 Å^2). MD simulations suggest that both $G\alpha_q$ and $G\alpha_i$ could stably bind to GLP-1R, albeit with a significantly reduced interface area (Supporting Information Fig. S5).

TMs 2−7 and intracellular loop 2 (ICL2) are the principal contributors to GLP-1R interaction with the Gα subunit, supplemented by minor contributions from helix 8 (H8) (Fig. 2A−C, Fig. S4E). The C-terminal tip of the Gα α5 helix is highly hydrophobic and inserted deeply into the intracellular crevice of GLP-1R, forming extensive hydrophobic contacts and polar interactions with TM5 and TM6 (Fig. 2B). Because $G\alpha_i$ carries a bulky C-terminal Phe (F354) rather than the corresponding Leu (L394) in $G\alpha_s$ or Val (V359) in $G\alpha_q$, alongside of the distinct side-chain orientation of R348$^{6.37b}$ (class B1 GPCR numbering in superscript) in GLP-1R TM6, the α5 helix in $G\alpha_i$ is distant from TM6 (Fig. 1I). This results in a markedly reduced interface area (219.3 Å^2) compared to $G\alpha_q$ (358.9 Å^2) and $G\alpha_s$ (302.1 Å^2) (Fig. S4E). The more extensive TM6−$G\alpha_q$ interface was reinforced by a polar network involving receptor residues R348$^{6.37b}$, K351$^{6.40b}$ and S352$^{6.41b}$ with N357, L358 and V359 of the α5 helix in $G\alpha_q$ (Fig. 2A, Supporting Information Table S2). Consequently, the R348$^{6.37b}$A substitution completely abolished G_q-mediated Ca^{2+} mobilization but only moderately reduced the potency (EC_{50}) of G_s-mediated cAMP accumulation (Fig. S4F and S4G, Supporting Information Table S3). In TM5, K334$^{5.64b}$ maintained polar contacts with all Gα subtypes through salt bridges and hydrophobic interactions (Fig. 2A), whereas N338$^{5.68b}$ formed hydrogen bonds with $G\alpha_s$ but showed weakened interaction with $G\alpha_i$ and $G\alpha_q$ (Table S2). Functionally, K334$^{5.64b}$A reduced GLP-1(7−36) elicited cAMP (with an 18% loss of E_{max} and 35-fold decrease in potency) and Ca^{2+} signaling (with a 62% loss of E_{max}), while N338$^{5.68b}$A selectively abolished Ca^{2+} mobilization while only moderately affecting cAMP accumulation, resulting in a 3-fold reduction in potency (Fig. S4F and S4G).

Polar contacts from TM2 and H8 further stabilized the α5 helix. In $G\alpha_q$, R176$^{2.46b}$ formed salt bridges with E355 of the α5 helix and with E408$^{8.49b}$ (Fig. 2A); in $G\alpha_s$ the interaction was realized by hydrogen bonds between R176$^{2.46b}$ and Q390, accompanied by contacts involving N406$^{8.47b}$/N407$^{8.48b}$ and E392. The results are supported by functional data: R176$^{2.46b}$A abolished Ca^{2+} mobilization and caused an 82-fold reduction in the potency of GLP-1(7−36) for cAMP accumulation, while N406$^{8.47b}$A and N407$^{8.48b}$A reduced potency in both cAMP accumulation and Ca^{2+} mobilization assays (Fig. S4F and S4G). Beyond these TMs, ICL2 and the adjacent region of TM3 adopted G protein subtype-dependent conformations (Fig. 2C). ICL2 had the largest interaction area with $G\alpha_s$ (417.2 Å^2), substantially greater than with $G\alpha_q$ (268.7 Å^2) or $G\alpha_i$ (207.6 Å^2) (Fig. S4E). L254$^{3.57b}$ made hydrophobic contacts with Y391 in $G\alpha_s$ and Y356 in $G\alpha_q$ but not with the equivalent C351 in $G\alpha_i$; it also interacted with H387 in $G\alpha_s$ but lacked the equivalent interactions in $G\alpha_q$ and $G\alpha_i$ (Fig. 2A and B). Consistent with these observations, L254$^{3.57b}$A abolished Ca^{2+} mobilization but only partially retained cAMP signaling (Fig. S4F and S4G).

Family-wide comparison of receptor−G protein interfaces shows that $G\alpha_s$ generally exhibits the largest interaction areas in class B1 GPCRs, ranging from 1684 Å^2 in parathyroid hormone 1 receptor (PTH1R) to 2382 Å^2 in glucagon receptor (GCGR), with a mean value of 1925 Å^2, significantly larger than the corresponding $G\alpha_q$ interfaces (1682 Å^2 for GLP-1R and 1392 Å^2 for PTH1R). In contrast, $G\alpha_i$ displays the smallest interface areas, such as 1282 Å^2 in GCGR and 1377 Å^2 in GLP-1R (Fig. 2D). These differences arise from distinct binding orientations and contact sets unique to each G protein subtype. Taking PTH1R as an example[13], although the C-terminal tips of the α5 helices from $G\alpha_q$ and $G\alpha_s$ overlap well within the intracellular crevice, the overall $G\alpha_q$ is oriented downward compared to $G\alpha_s$, with the αN helix shifted by 4.42 Å and the N-terminal region of α5 shifted by 2.91 Å (Figs. 1F and 2C, Fig. S4C). Similar movements were observed when comparing G_i- and G_s-coupled GCGR complexes (Figs. 1H and 2C, Fig. S4D). These positional differences primarily stem from sequence variations in the α5 helix across $G\alpha_q$, $G\alpha_s$, and $G\alpha_i$, which interact extensively with ICL2, TM5, and TM6, thereby influencing the entry position and orientation of the Gα (Fig. 2B). Notably, receptor-specific adaptations are most evident in ICL2 (Fig. 2C). In GCGR, ICL2 underwent substantial rearrangement when switching between G_i- and G_s-coupled states, reflecting considerable conformational flexibility[14]. In contrast, GLP-1R and PTH1R displayed obvious rigidity in ICL2 through side-chain reorientations, allowing for G protein accommodation

1R in deep sky blue, $G\alpha_q$ in hot pink, Gβ in yellow, and Gγ in chartreuse. (D) Cryo-EM density map (left) and cartoon representation (right) of GLP-1-bound GLP-1R coupled to G_i, with the sharpened cryo-EM density map shown at a threshold of 0.025. The peptide GLP-1 is displayed in saddle brown, GLP-1R in cornflower blue, $G\alpha_i$ in salmon, Gβ in yellow, Gγ in chartreuse, and scFv16 in light gray. (E) Superimposition of G_q- and G_s-coupled (PDB code: 6X18) GLP-1−GLP-1R complex structures. (F) Superimposition of the G_q-coupled (PDB code: 9JR2) and G_s-coupled (PDB code: 8FLQ) structures of the PTH−PTH1R complex. (G) Superimposition of the G_i- and G_s-coupled GLP-1−GLP-1R complex structures. (H) Superimposition of the G_i-coupled (PDB code: 6LML) and G_s-coupled (PDB code: 6LMK) glucagon (GCG)−GCGR complex structures. Close-up views from the intracellular perspective illustrate the conformation of the transmembrane helical bundle of receptor and the positioning of the α5 helix at the C terminus of Gα, shown in cartoon representation. (I) Structural comparison of GLP-1R engagement by the C-terminal tip of the Gα α5 helix across G_s, G_q, and G_i proteins.

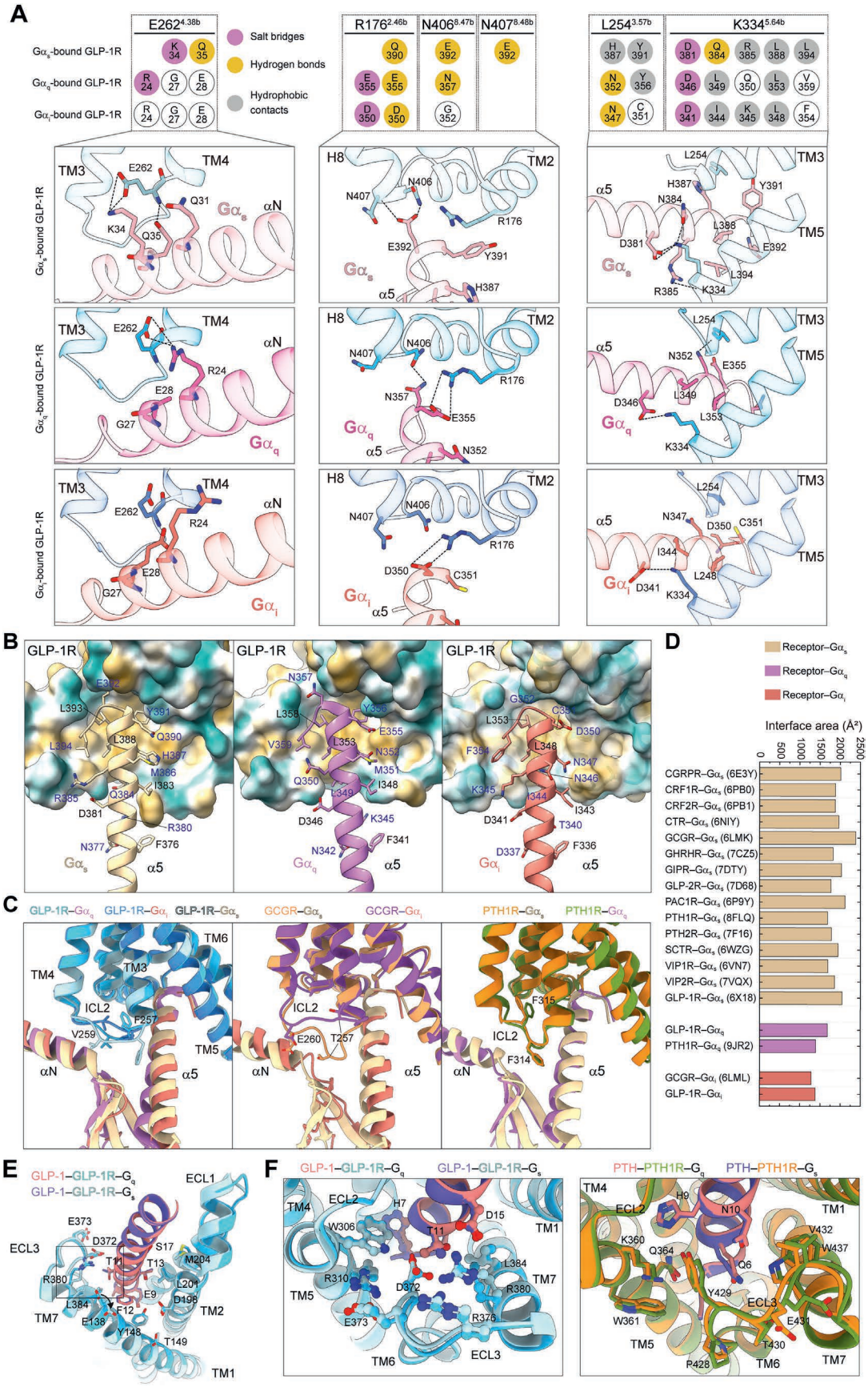
A
Salt bridges
Hydrogen bonds
Hydrophobic contacts
B
C
D
Receptor–Gαs
Receptor–Gαq
Receptor–Gαi
Interface area (Å²)
CGRPR–Gαs (6E3Y)
CRF1R–Gαs (6PB0)
CRF2R–Gαs (6PB1)
CTR–Gαs (6NIY)
GCGR–Gαs (6LMK)
GHRHR–Gαs (7CZ5)
GIPR–Gαs (7DTY)
GLP-2R–Gαs (7D68)
PAC1R–Gαs (6P9Y)
PTH1R–Gαs (8FLQ)
PTH2R–Gαs (7F16)
SCTR–Gαs (6WZG)
VIP1R–Gαs (6VN7)
VIP2R–Gαs (7VQX)
GLP-1R–Gαs (6X18)
GLP-1R–Gαq
PTH1R–Gαq (9JR2)
GCGR–Gαi (6LML)
GLP-1R–Gαi
E
F

via minimal structural changes rather than large-scale rearrangements (Fig. 2C). Structural superposition of these GLP-1R complexes with the closely related glucose-dependent insulinotropic polypeptide receptor (GIPR) in its G_s-bound state reveals a conserved intracellular architecture, suggesting that GIPR is structurally capable of accommodating different G protein subtypes (Supporting Information Fig. S6). However, sequence variations at key interfacial positions (*e.g.*, R328 and F345 in GIPR) and conformational differences in ICL2 are observed, which likely give rise to distinct side-chain packing and interaction networks (Fig. S6) and may contribute to the unique G protein coupling selectivity profile of GIPR. Taken together, the results highlight a mechanistic explanation in which G protein subtype selectivity arises from differences in α5 helix positioning and orientation, facilitated either by a modest ICL2 flexibility (as in GCGR) or by fine-grained side-chain adjustments (as in GLP-1R and PTH1R).

Despite substantial conformational differences at the G protein-coupling interface, the extracellular region of GLP-1R and the bound GLP-1 were well aligned across the three complexes (G_s-, G_i- and G_q-coupled states), a pattern that was also observed in GCGR and PTH1R complexes (Fig. 2E, Fig. S7A and S7B)[13,14]. However, several side-chains adopted different orientations depending on the bound Gα subtype (G_s, G_q or G_i) such as $E138^{1.33b}$, $D372^{ECL3}$ and $R380^{7.35b}$ (Fig. 2F). Mechanistically, GLP-1 binding is accompanied by an inward movement of the extracellular half of TM1 and an outward movement of TM7, which together create a binding site for the peptide N-terminus. Concurrently, a conformational transition of ECL1 further stabilizes the C-terminus of GLP-1 (Supporting Information Fig. S8).

ECL3 functioned as a structural and functional hub linking extracellular peptide recognition to intracellular G protein accommodation. Outward displacement of ECL3 upon GLP-1 binding permitted the formation of a polar network at the receptor−peptide interface ($W306^{5.36b}$−$D372^{ECL3}$−$R380^{7.35b}$−$D15^{GLP-1}$) and, concomitantly, promoted positional adjustments of TM5 and TM6 on the intracellular side (Fig. 2F). This coupled extracellular-intracellular rearrangement creates a coordinated regulatory axis that may facilitate insertion of the Gα α5 helix (Fig. S8). Minor side-chain reorientations within this axis (*e.g.*, like $D372^{ECL3}$ and $R380^{7.35b}$) were observed among Gα subtypes and may fine tune the interface (Fig. 2F). These local changes were stabilized by a TM5−ECL3 salt bridge ($R310^{5.40b}$−$E373^{ECL3}$) in both G_s- and G_q-bound states. Consistent with this mechanism, functional perturbation of the ECL3−TM5 network selectively impaired G_q signaling: $D372^{ECL3}$N, $E373^{ECL3}$Q and $R380^{7.35b}$Q completely abolished Ca^{2+} mobilization. However, these mutants retained their ability to elicit G_s-mediated cAMP signaling with greatly reduced potency (Fig. S7C and S7D). Thus, formation of the ECL3−TM5−GLP-1 polar network may be associated with G protein subtype discrimination. Extending this principle to small-molecule GLP-1R agonist, we observe that extracellular conformational changes induced by danuglipron (PF-06882961) and TT-OAD2 diverge significantly within the ECL3 region (Supporting Information Fig. S9). These ligand-specific structural alterations at the ECL3−TM7 interface likely provide a direct physical correlation with their divergent signaling biases, indicating that allosteric modulation of this extracellular nexus underlies biased signaling across diverse chemotypes. Notably, this model of ECL3 serving as an allosteric nexus appears to extend to other class B1 GPCRs. For instance, a comparative analysis of PTH1R structures coupled to G_s versus G_q reveals that while the overall architecture of the TM6−ECL3−TM7 interface with bound PTH is conserved, distinct side-chain conformations (particularly at E431) and backbone displacements (especially within ECL3) are evident. These structural differences, correlated with distinct intracellular G protein subtype, further demonstrate how alterations in the intracellular binding partner can allosterically propagate conformational changes that are discernible at the extracellular ligand-binding region (Fig. 2F).

Examination of TM1, TM2 and ECL1 which form extensive contacts with GLP-1 shows that the peptide and receptor backbones were well aligned, while several side-chains adopted subtle orientation differences (Fig. 2F). For example, the side-chain of $E138^{1.33b}$ positioned closer to G_q-bound GLP-1 than that of G_s-bound; $E138^{1.33b}$R markedly impaired G_q-mediated Ca^{2+} influx but had tolerable effect on G_s-mediated cAMP signaling (Fig. S7C and S7D). Another key determinant at the receptor−peptide interface is $L201^{2.71b}$ in TM2, which inserted into a hydrophobic patch formed by $T13^{GLP-1}$, $V16^{GLP-1}$, $K197^{2.67b}$, $M204^{2.74b}$ and $F230^{3.33b}$. Replacement of L201 with a larger hydrophobic residue ($L201^{2.71b}$M) fully abolished peptide-induced Ca^{2+} mobilization; G_s-mediated cAMP accumulation is severely affected but not eliminated (36% loss of E_{max} and 109-fold decrease in potency) (Fig. S7C and S7D). Together, our results suggest that the binding pocket exerts residue-level control over biased signaling.

GLP-1R exhibits inherent effector coupling promiscuity—engaging G_s, G_q, G_i and β-arrestins to drive pleiotropic metabolic responses—yet the structural determinants governing its differential G protein selectivity remain unknown. Through high-resolution structural analysis of GLP-1R−G protein complexes and functional studies, we reveal that the TMD of GLP-1R adopts a highly conserved active conformation capable of accommodating G_q, G_i, and G_s subtypes. In contrast, the Gα subunits themselves display significant structural variations, particularly within the αN and α5 helices, leading to distinct binding modes and a reduced interface area, especially pronounced in the case of G_i compared to G_s. Functional mutagenesis data support a model in which biased signaling is regulated through two interconnected mechanisms: intracellular regions (including TM segments and ICLs) that

Figure 2 Molecular basis of G protein coupling preference of GLP-1R. (A) Comparison of the interactions between GLP-1R and three G protein α subunits ($G\alpha_s$, $G\alpha_q$ and $G\alpha_i$), described by fingerprint strings encoding different interaction types of the surrounding residues. Close-up views of these interactions are shown with polar contacts depicted as black dashed lines. G protein residues are colored by interaction type: purple (salt bridge), yellow (hydrogen bond) and gray (hydrophobic interactions). (B) Binding pocket for the α5 helices of Gα subunits, with GLP-1R shown in surface representation. Residues within the α5 helix that are sequence-divergent across Gα subtypes are highlighted in blue. (C) Conformational comparison of ICL2 in distinct G protein subtype coupled states of GLP-1R (left), GCGR (middle) and PTH1R (right). (D) Comparison of receptor−Gα interface areas across class B1 GPCRs, calculated using FreeSASA. (E) Close-up view of the GLP-1-binding conformation at the extracellular halves of GLP-1R coupled to different G proteins. The ECD was omitted for clarity. (F) Conformational variation at the TM6−ECL3−TM7−peptide interface between G_s- and G_q-coupled complex structures of GLP-1R (left) and PTH1R (right). The G_q-coupled (PDB code: 9JR2) and G_s-coupled (PDB code: 8FLQ) structures of the PTH−PTH1R complex are shown.

establish subtype-specific contacts with Gα, and extracellular elements—notably ECL3 and TM1−TM2—that allosterically modulate intracellular coupling. This structural framework explains how a single agonist can promote divergent signaling outcomes and how localized alterations, whether in ligand chemistry or peptide modification, can induce significant bias in downstream responses[15]. This extracellular-to-intracellular coupling axis aligns with prior findings that peptide N-terminal interactions and dynamics with the GLP-1R TMD influence G protein activation kinetics and efficacy[16]. Furthermore, ligand-specific signaling signatures (including conformation, functional selectivity, and location bias) for GLP-1R agonists are correlated with distinct cellular and clinical outcomes[17]. The atomic-level structural variations reported here provide a direct mechanistic basis for understanding such differential signaling profiles. For instance, ligand interactions at the extracellular allosteric networks (*e.g.*, the ECL3 polar network) can allosterically reshape the intracellular coupling interface, thereby shifting response toward specific G protein subtypes and signaling compartments. Future structural studies of biased peptide in complex with GLP-1R and distinct G protein subtypes/arrestins will further elucidate these principles, advancing the strategy of achieving pathway selectivity. Collectively, our findings offer a residue-level understanding of G protein subtype selectivity and furnish a structural blueprint for designing biased agonists at GLP-1R, and possibly at other class B1 GPCRs.

Acknowledgements

We are grateful to Yiting Mai, Wenbo Feng, Yan Chen and Zhaotong Cong for technical assistance. This work was partially supported by the National Natural Science Foundation of China (82273961, 82073904, and 81872915 to Ming-Wei Wang), STI2030-Major Project 2021ZD0203400 (to Qingtong Zhou, China), and Hainan Provincial Major Science and Technology Project ZDKJ2021028 (to Dehua Yang and Qingtong Zhou, China). The cryo-EM data were collected at Cryo-Electron Microscopy Research Center and Advanced Center for Electron Microscopy, Shanghai Institute of Materia Medica, Chinese Academy of Sciences.

Author contributions

Qingtong Zhou, Jie Li, Yao Zhang, Xiaoqing Cai and Wei Han performed research; Qingtong Zhou, Jie Li, Yao Zhang, Wei Han and Ming-Wei Wang analyzed the data; Xiaoqing Cai conducted calcium mobilization assay and analyzed the results under the supervision of Dehua Yang; Qingtong Zhou, Jie Li, Yao Zhang and Ming-Wei Wang wrote the manuscript with inputs from all coauthors; Ming-Wei Wang initiated the project and supervised the studies.

Conflicts of interest

The authors declare that there is no conflict of interest.

Data availability

All relevant structure data are available from the authors and/or included in the manuscript or Supporting Information. The atomic coordinates and electron microscopy maps have been deposited in the Protein Data Bank (PDB) under accession codes: 9X22 (GLP-1−GLP-1R−G_q complex) and 9X20 (GLP-1−GLP-1R−G_i complex), as well as Electron Microscopy Data Bank (EMDB) under accession codes: EMD-66470 (GLP-1−GLP-1R−G_q complex) and EMD-66468 (GLP-1−GLP-1R−G_i complex). All relevant data are available from the authors and/or included in the manuscript or Supporting Information.

Appendix A. Supporting information

Supporting information to this article can be found online at https://doi.org/10.1016/j.apsb.2026.01.023.

References

1. Drucker DJ. Mechanisms of action and therapeutic application of glucagon-like peptide-1. *Cell Metab* 2018;**27**:740−56.
2. Zheng Z, Zong Y, Ma Y, Tian Y, Pang Y, Zhang C, et al. Glucagon-like peptide-1 receptor: mechanisms and advances in therapy. *Signal Transduct Target Ther* 2024;**9**:234.
3. Zhou Q, Zhao F, Zhang Y, Yang D, Wang MW. Structural pharmacology and mechanisms of GLP-1R signaling. *Trends Pharmacol Sci* 2025;**46**:422−36.
4. Oduori OS, Murao N, Shimomura K, Takahashi H, Zhang Q, Dou H, et al. Gs/Gq signaling switch in beta cells defines incretin effectiveness in diabetes. *J Clin Investig* 2020;**130**:6639−55.
5. Gao Y, Ryu H, Lee H, Kim YJ, Lee JH, Lee J. ER stress and unfolded protein response (UPR) signaling modulate GLP-1 receptor signaling in the pancreatic islets. *Mol Cells* 2024;**47**:100004.
6. Jones B, Buenaventura T, Kanda N, Chabosseau P, Owen BM, Scott R, et al. Targeting GLP-1 receptor trafficking to improve agonist efficacy. *Nat Commun* 2018;**9**:1602.
7. McNeill SM, Lu J, Marion CCC, Inoue A, Zhao P, Sexton PM, et al. The role of G protein-coupled receptor kinases in GLP-1R beta-arrestin recruitment and internalisation. *Biochem Pharmacol* 2024;**222**:116119.
8. Marzook A, Tomas A, Jones B. The interplay of glucagon-like peptide-1 receptor trafficking and signalling in pancreatic beta cells. *Front Endocrinol* 2021;**12**:678055.
9. Moo EV, Moller TC, Sorensen FA, Inoue A, Brauner-Osborne H. Arrestin-independent internalization of the GLP-1 receptor is facilitated by a GRK, clathrin, and caveolae-dependent mechanism. *FEBS J* 2025;**292**:1675−95.
10. Zhang Y, Sun B, Feng D, Hu H, Chu M, Qu Q, et al. Cryo-EM structure of the activated GLP-1 receptor in complex with a G protein. *Nature* 2017;**546**:248−53.
11. McLean BA, Wong CK, Campbell JE, Hodson DJ, Trapp S, Drucker DJ. Revisiting the complexity of GLP-1 action from sites of synthesis to receptor activation. *Endocr Rev* 2021;**42**:101−32.
12. Zhang X, Belousoff MJ, Zhao P, Kooistra AJ, Truong TT, Ang SY, et al. Differential GLP-1R binding and activation by peptide and non-peptide agonists. *Mol Cell* 2020;**80**:485−500.e7.
13. Sano FK, Shimizume K, Kobayashi K, Awazu T, Kawakami K, Akasaka H, et al. Insights into G-protein coupling preference from cryo-EM structures of G_q-bound PTH1R. *Nat Chem Biol* 2025;**12**:1906−14.
14. Qiao A, Han S, Li X, Li Z, Zhao P, Dai A, et al. Structural basis of G_s and G_i recognition by the human glucagon receptor. *Science* 2020;**367**:1346−52.
15. Wootten D, Reynolds CA, Smith KJ, Mobarec JC, Koole C, Savage EE, et al. The extracellular surface of the GLP-1 receptor is a molecular trigger for biased agonism. *Cell* 2016;**165**:1632−43.
16. Deganutti G, Liang YL, Zhang X, Khoshouei M, Clydesdale L, Belousoff MJ, et al. Dynamics of GLP-1R peptide agonist engagement are correlated with kinetics of G protein activation. *Nat Commun* 2022;**13**:92.

17. Wright SC, Motso A, Koutsilieri S, Beusch CM, Sabatier P, Berghella A, et al. GLP-1R signaling neighborhoods associate with the susceptibility to adverse drug reactions of incretin mimetics. *Nat Commun* 2023;**14**:6243.

Qingtong Zhou[a,b,†], Jie Li[c,†], Yao Zhang[c], Xiaoqing Cai[d,e], Wei Han[a], Dehua Yang[b,d,e], Ming-Wei Wang[a,b,c,f,g,*]

[a]*Research Center for Medicinal Structural Biology, National Research Center for Translational Medicine at Shanghai, State Key Laboratory of Medical Genomics, Ruijin Hospital, Shanghai Jiao Tong University School of Medicine, Shanghai 200025, China*

[b]*Research Center for Deepsea Bioresources, Sanya 572025, China*

[c]*Department of Pharmacology, School of Basic Medical Sciences, Fudan University, Shanghai 200032, China*

[d]*The CAS Key Laboratory of Receptor Research, Shanghai Institute of Materia Medica, Chinese Academy of Sciences, Shanghai 201203, China*

[e]*The National Center for Drug Screening, Shanghai Institute of Materia Medica, Chinese Academy of Sciences, Shanghai 201203, China*

[f]*Engineering Research Center of Tropical Medicine Innovation and Transformation of Ministry of Education, School of Pharmacy, Hainan Medical University, Haikou 570228, China*

[g]*Department of Chemistry, School of Science, The University of Tokyo, Tokyo 113-0033, Japan*

*Corresponding author.
E-mail address: mwwang@simm.ac.cn (Ming-Wei Wang)

[†]These authors made equal contributions to this work.

Received 11 December 2025
Received in revised form 22 December 2025
Accepted 15 January 2026